Roles of silver nanoclusters in surface-enhanced Raman spectroscopy

Takao Tsuneda[1],* Takeshi Iwasa[2,3], and Tetsuya Taketsugu[2,3]

[1]*Graduate School of Science, Technology, and Innovation, Kobe University, Kobe 657-8501, Japan*

[2]*Department of Chemistry, Faculty of Science, Hokkaido University, Sapporo 060-0810, Japan and*

[3]*Institute for Chemical Reaction Design and Discovery (WPI-ICReDD), Hokkaido University, Sapporo 001-0021, Japan*

Abstract

The cause for the huge enhancement factors of surface-enhanced Raman spectroscopy (SERS) by the addition of small silver nanoclusters is theoretically investigated focusing on the difference between resonance Raman activity and surface plasmon effects. First, the resonance and off-resonance Raman spectra are calculated using the incident light wavenumbers of the low-lying charge transfer excitations for the surface (S) and vertex (V) complexes of pyridine molecule attaching to three small silver nanoclusters: Ag_5, Ag_{10} and Ag_{20}. As a result, it is found that the incident radiation dramatically increases the resonance Raman activities with the enhancement factors up to 10^{12}. This indicates that the resonance Raman effects are dominant in the enhancement factors of SERS, at least when to use small silver clusters. It is also found that the resonance Raman spectra significantly depend on the adsorption sites given in S or V complexes, and on the inclusion or exclusion of the long-range correction for density functional theory, irrespective of the size of the silver clusters. The electromagnetic field enhancement effects called "surface plasmon effects" are also examined for the Ag_{20} cluster to confirm this conclusion. Consequently, the enhancement in the electric field are roughly evaluated as less than one for the static polarizability of this small cluster. It is, therefore, concluded that the resonance Raman activity effect is dominant in the huge SERS enhancement factors for, at least, small silver nanoclusters.

I. INTRODUCTION

Surface plasmon[1,2] is a quantized collective oscillation of electrons, which appear in the surface of metal crystals and metal nanoparticles. It has long attracted attentions due to its potential in the advancement of nanoscience.[3–5] For example, the propagation of the surface plasmon is often investigated in the field of photonics as a possible information carrier.[6] The surface plasmon effect has been investigated combining with scanning tunneling microscopic techniques to potentiate its spectroscopic measurement in the size-regime down to single-molecule scale.[7–9] Many theoretical studies have so far been performed to make clear the roles of the surface plasmon in these applications.[10,11] In the field of chemistry, the surface plasmon resonance has also been intensively studied due to the anticipated significant role in the remarkable enhancement of resonance Raman scattering cross sections, which pave the way for single-molecule-scale spectroscopies and microscopies. It is known that silver and gold clusters dramatically enhance the Raman scattering cross sections of the latter of adsorbed molecules by 10^7 to 10^{12} times and have led to the development of surface-enhanced Raman spectroscopy (SERS).[12] In SERS, the surface plasmon has been explained to affect this enhancement through the significant increase in the local intensity of the incident light.

The surface plasmon effect on the incident light is evaluated by calculating the induced local polarizabilities inside supported metal clusters and then solving the Maxwell equation to obtain enhanced local electric fields. There are several methods to calculate the local electric fields: e.g., the discrete dipole approximation (DDA) method[13] and the finite-difference time-domain (FDTD) method.[14,15] For nanostructures with non-spherical geometry, using the DDA method, Schatz and coworkers calculated the enhancement factors for the Raman scattering cross sections of the pyridine-silver icosamer (Ag_{20}) complex, and consequently, evaluated them in the region of 10^4 to 10^5.[16] Note, however, that, since the silver icosamer is too small to be metallic with a considerable band gap, this result seems inconsistent with conventional experimental results showing that only large metallic metal clusters provide surface plasmon effects. Actually, a recent experimental study showed that for thiolate-protected gold clusters, the 246-mer (Au_{246}) is non-metallic (i.e., molecular) whereas 279-mer (Au_{279}) is metallic.[17] A subsequent theoretical study on the 279-mer showed that the only absorption band, which is usually interpreted as a surface plasmon resonance excitation, is obtained in the time-dependent (TD) response density functional theory (DFT)[18] calculation of this

cluster.[19] This indicates that the surface plasmon comes from the zero band gaps of metallic electronic structures. Using the DDA method, Xu et al. also calculated the squared enhancement factors, $|E|^2 / |E_0|^2$, of large gold/silver core/shell nanospheres with the core range from 10 to 40 nm and the shell thickness ranges from 1 to 11 nm.[20] They consequently obtained the squared enhancement factors as only 180, which is much smaller than the experimental enhancement factors. This indicates that the surface plasmon effects are too small to affect the Raman spectra even for small metal nanoclusters and the immense enhancement factors are attributed to other causes.

Schatz and co-workers[16] also calculated the enhancement factors of the resonance Raman cross sections, which are called "chemical enhancement", through the polarizabilities induced by the electron transfer from the icosamer to the pyridine molecule using DFT with a generalized-gradient-approximation (GGA)-type functional. Consequently, they evaluated the enhancement factors in the region of 10^3 to 10^6. The cross section depends on the incident light wavenumber to the fourth power and the polarizability and anisotropy to the second power, while the incident light irradiation increases the polarizability and anisotropy (see Sec. II). Note that long-range charge transfer (CT) excitations induce huge polarizabilities and anisotropies in molecules. It is established that the long-range correction (LC)[21–23] is required for GGA functionals to calculate CT excitation energies.[24] This indicates that LC should be incorporated to investigate the resonance Raman cross sections in DFT calculations, though it has been taken into consideration only in a few studies.[25]

Recently, one of the authors theoretically investigated the electronic states of small silver nanoclusters.[26] As a result, it was found that LC-GGA[21–23] quantitatively reproduces the HOMO-LUMO gaps of the small silver nanoclusters, which are the difference between the minus vertical ionization potentials (VIPs) and the minus vertical electron affinities (VEAs) and are usually much larger than the HOMO-LUMO excitation energies for small clusters. This is contrasting to the result that Perdew-Burke-Ernzerhof (PBE)[27] GGA functional seriously underestimate the HOMO-LUMO gaps, while it provides accurate HOMO-LUMO excitation energies close to those of LC-DFT in TDDFT calculations. This indicates that the exciton binding energies, i.e., the difference between the orbital energy gaps and corresponding excitation energies, mainly come from the long-range exchange interactions and they play a significant role in the electronic states of small silver nanoclusters. Since electron excitations mainly contribute to the peak enhancement of resonance Raman spectra,

this also indicates that LC should be included in DFT calculations to explore the SERS enhancement factors. This study also shows that the least-squares fits of the calculated VIPs and VEAs to a function, $f(n) = a + bn^{-c}$ (n is the number of atoms and a, b and c are real numbers) suggest that the VIP-VEA values, i.e., the HOMO-LUMO gaps, become zero with $n \approx 300$ and 500 for LC-DFT and PBE, respectively. Several hundred silver atoms are, therefore, required to make silver clusters metallic in DFT calculations irrespective of the functional used. Considering that the surface plasmon comes from the zero band gaps of metallic electronic structures,[19] these studies cast doubts on that surface plasmon effects cause huge enhancement factors even for nonmetallic small silver nanoclusters.

In this study, the cause for the huge SERS enhancement factors, which are induced by doping small silver nanoclusters, are theoretically investigated for the adsorption of pyridine molecule on the small silver nanoclusters. In particular, we focus on the long-range exchange effects on the SERS enhancement by comparing the results of LC-GGA and PBE functionals. The surface plasmon effects on Ag_{20} cluster are also examined to compare the effect on the SERS enhancement factors for the use of small silver nanoclusters.

II. COMPUTATIONAL DETAILS

Geometry optimizations have been performed for the models of pyridine molecule on three types of small silver clusters, i.e., Ag_5, Ag_{10} and Ag_{20}, in which surface (S) and vertex (V) complexes are examined following the study of Schatz and coworkers[16] for comparison (Fig. 1). The Kohn-Sham calculations[28,29] have been carried out using the long-range correction (LC)[21,22] of Becke 1988 exchange[30] plus Lee-Yang-Parr correlation[31] (BLYP) functional (the only parameter $\mu = 0.33$[24]). The BLYP and hybrid B3LYP GGA[32] calculations also have been examined to make clear the long-range exchange effects. The cc-pVDZ basis set[33,34] was used for H, C and N atoms and LANL2DZ effective core potential basis set[35] was employed for Ag atom. Note that the high reliability of the combination of this method and basis set has been confirmed in the previous calculation of silver clusters.[26] For the optimized structures, it was found that the V-complexes are more stable than the S-complexes by 3.70, 0.32 and 7.60 kcal/mol for Ag_5, Ag_{10} and Ag_{20}, respectively. The response time-dependent Kohn-Sham (TDKS)[18] calculations also have been performed to obtain the low-lying excitation energies of these complexes.

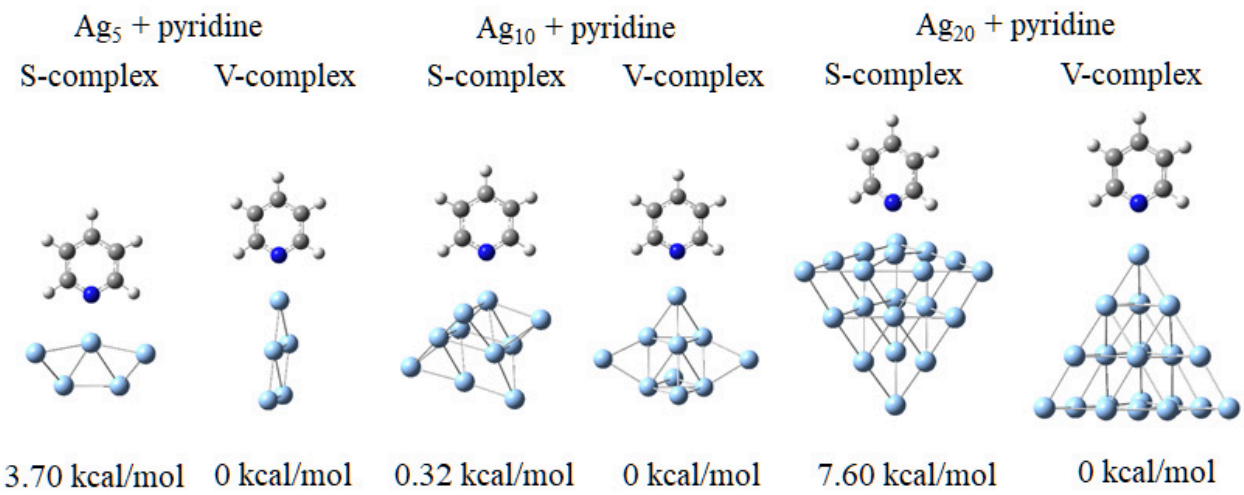

FIG. 1: Optimized geometries of silver cluster models, Ag_5, Ag_{10} and Ag_{20}, attaching pyridine molecule for the S- and V-complex structures with the energy differences. LC-BLYP/cc-pVDZ is used.

Using the (incident light) wavenumbers corresponding to the low-lying CT excitations, resonance Raman activity calculations have been carried out. As the Raman scattering intensity, the differential scattering cross section, i.e., the ratio of scattering cross section $d\sigma$ in a conical beam of solid angle $d\Omega$, $d\sigma/d\Omega = I(\theta = \pi/2)/\Im N_{\rm tot}$ (I is the genuine Raman scattering intensity with the angle of propagation of the incident beam and the direction of observation θ and $N_{\rm tot}$ is the total number of molecules), is used to avoid the dependence on the irradiance $\Im$. The differential scattering cross section is evaluated as (in atomic unit)[36]

$$\frac{d\sigma}{d\Omega} = \frac{\pi^2}{\epsilon_0^2}\left(\tilde{\omega}_{\rm in} - \tilde{\omega}_p\right)^4 \frac{1}{4\pi c\tilde{\omega}_p}\left(\frac{45\alpha_p'^2 + 7\gamma_p'^2}{45}\right)\frac{1}{1-\exp\left[-2\pi c\tilde{\omega}_p/k_{\rm B}T\right]}, \tag{1}$$

where ϵ_0 is the vacuum permittivity and $\tilde{\omega}_{\rm in}$ and $\tilde{\omega}_p$ are the wavenumbers of the incident

beam and the vibrational transition for normal mode p, respectively. In Eq. (1), α_p' is the mean isotropic polarizability derivative for the p-th normal mode,

$$\alpha_p' = \frac{1}{3}\left\{\left(\bar{\alpha}_{xx}'\right)_p + \left(\bar{\alpha}_{yy}'\right)_p + \left(\bar{\alpha}_{zz}'\right)_p\right\}, \tag{2}$$

and γ_p' is the anisotropy of the polarizability derivative matrix for the p-th mode,

$$\begin{aligned}\gamma_p' = \; & \frac{1}{2}\left\{\left[\left(\bar{\alpha}_{xx}'\right)_p - \left(\bar{\alpha}_{yy}'\right)_p\right]^2 + \left[\left(\bar{\alpha}_{yy}'\right)_p - \left(\bar{\alpha}_{zz}'\right)_p\right]^2 + \left[\left(\bar{\alpha}_{zz}'\right)_p - \left(\bar{\alpha}_{xx}'\right)_p\right]^2\right. \\ & \left. +6\left[\left(\bar{\alpha}_{xy}'\right)_p^2 + \left(\bar{\alpha}_{yz}'\right)_p^2 + \left(\bar{\alpha}_{zx}'\right)_p^2\right]\right\}. \end{aligned} \tag{3}$$

In Eq. (3), $\left(\bar{\alpha}'_{rs}\right)_p$ is the polarizability derivative variation with respect to the normal modes,

$$\left(\bar{\alpha}'_{rs}\right)_p = \left(\frac{\partial \bar{\alpha}_{rs}}{\partial \mathbf{R}_p}\right), \tag{4}$$

where $\bar{\alpha}_{rs}$ is the rs-component of the polarizability of the molecule. and $\mathbf{R}_p$ is the p-th mode of the normal coordinates of the molecule. The off-resonance Raman activity calculations have also been done using static polarizability derivatives.

The Gaussian 09 suite of program[37] has been used to perform the geometry optimizations and the resonance Raman calculations. All of the optimized structures have been checked to ensure that they yield positive, real frequencies. The calculated Raman spectra have been analyzed using GaussView 5.0.8.[38]

To explore the field enhancement effect of Ag_{20} cluster, the enhancement factor of the electric field has also been calculated. The induced electric field, $\boldsymbol{E}^{\mathrm{ind}}$, is estimated for the Ag_{20} cluster by using the dipolar field as expressed by the next formula.[39]

$$\boldsymbol{E}^{\mathrm{ind}}(\boldsymbol{r}) = \frac{[3\boldsymbol{n}(\boldsymbol{n}\cdot\boldsymbol{d}) - \boldsymbol{d}]}{r^3} e^{-ikr}, \tag{5}$$

where k is a wavenumber and $\boldsymbol{n}$ is the unit vector of $\boldsymbol{r}/r$. The induced dipole moment $\boldsymbol{d}$ is represented using the polarizability $\alpha(\omega)$ and incident field $\boldsymbol{E}^0$ as

$$\boldsymbol{d} = \alpha(\omega)\boldsymbol{E}^0 = \alpha(\omega)\hat{\boldsymbol{e}}^0|\boldsymbol{E}^0|, \tag{6}$$

where $\hat{\boldsymbol{e}}^0$ is the unit vector of $\boldsymbol{E}^0/|\boldsymbol{E}^0|$. Combining Eqs. (5) and (6) gives

$$\boldsymbol{E}^{\mathrm{ind}}(\boldsymbol{r})/|\boldsymbol{E}^0| = \frac{\alpha(\omega)}{r^3} \times \left[3\boldsymbol{n}(\boldsymbol{n}\cdot\hat{\boldsymbol{e}}^0) - \boldsymbol{e}^0\right]. \tag{7}$$

Considering that the incident light is in the UV-Vis region, e^{-ikr} in Eq. (5) can be approximated to be ~ 1. The static and dynamic polarizabilities of Ag_{20} have also been calculated for the excited states, which are calculated using resolution of identity (RI) approach to B3LYP functional[31,32] with def-SV(P) basis set[40] under the resolution of the identity approximation for the Coulomb integral[41] as implemented in TURBOMOLE suite of program.[42,43]

III. RESULTS AND DISCUSSIONS

A. Off-resonance and resonance Raman spectra of pyridine on Ag_{20} complex

We first explored the difference between off-resonance and resonance Raman spectra for the S- and V-complexes of pyridine molecule on Ag_{20} cluster. Figure 2 illustrates the calculated Raman spectra, in which each peak with frequency ν is multiplied by the Gaussian distribution function:

$$f(\nu) = \frac{1}{\sqrt{2\pi\sigma^2}} \exp\left[-\frac{(\nu-\mu)^2}{2\sigma^2}\right], \tag{8}$$

where σ is the standard deviation ($\sigma = 5$ is set in this study) and μ is the peak frequency. Note that this figure shows only the resonance Raman spectra of the lowest CT excitations of the complexes in TDKS calculations: i.e., 280.93 and 393.90 nm for S- and V-complexes, respectively.

Figure 2 shows that the Raman spectrum peaks for the wavelengths of 300 through 1800 cm^{-1} correspond to the peaks of pyridine molecule, and the off-resonance and resonance Raman spectra give very different strong peak positions for both S- and V-complexes. The highest peaks at 1225 and 1510 cm^{-1} in the resonance Raman spectrum of the V-complex correspond to the axial symmetric C-H and C-C stretchings and asymmetric C-H stretchings of pyridine molecule, respectively, while those at 1220 and 1685 cm^{-1} in that of the S-complex correspond to the symmetric in-plane C-H stretchings and axial symmetric C-H and C-C stretchings of pyridine molecule, respectively.[44–47] Since Raman spectrum peak intensities are proportional to the polarizability variations for the vibration modes, the Raman peaks of the axial vibrations are mainly amplified after the CT excitations. The discrepancy in the Raman spectra of the S- and V-complexes is attributed to the difference in the effects of the axial and its in-plane perpendicular vibrations of pyridine molecule on the electronic states of the complexes after the CT excitations. Based on Eq. (1), this indicates that the electric field, which are evaluated to induce CT in TDKS calculations, significantly change the polarizability and/or anisotropy variations by the normal modes of molecules. This is because another incident light-dependent term, i.e., $(\tilde{\omega}_{\rm in} - \tilde{\omega}_p)^4$ term, simply vary the cross section independent of the normal modes. Note that these discrepancies are also found in the experimental resonance Raman spectra.[5]

The figure also shows that the S- and V-complexes provide very different resonance Ra-

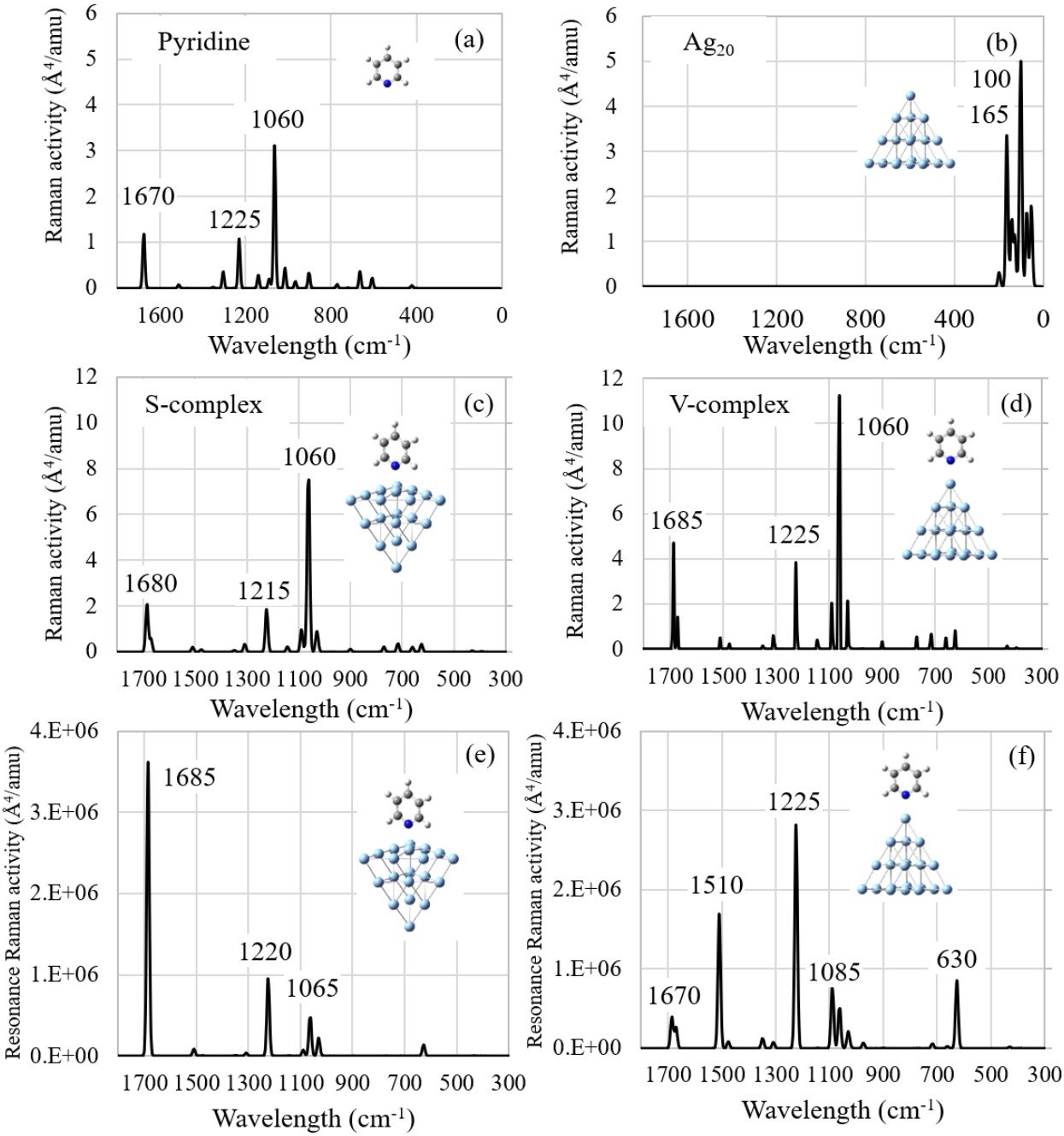

FIG. 2: Calculated on/off-resonance Raman spectra of pyridine@Ag_{20} complexes: (a) and (b) correspond to the off-resonance Raman spectra of pyridine molecule and Ag_{20} cluster, (c) and (d) correspond to the off-resonance Raman spectra of the S- and V-complexes and (e) and (f) correspond to the resonance ones of the S- and V-complexes, respectively. All the peaks are multiplied by the Gaussian distribution function. For (e) and (d), the spectra correspond to the lowest charge transfer excitations of the complexes, for which the wavelengths of 280.93 and 393.90 nm for S- and V-complexes, respectively. LC-BLYP/cc-pVDZ is used.

man spectra, though they give similar off-resonance Raman spectra for, at least, the peak positions. This suggests that the polarizability and/or anisotropy variations significantly depend on the adsorption sites under the irradiation. Note that the Raman spectrum peaks in the region of this figure from 300 through 1800 cm^{-1} correspond to the normal modes of pyridine molecule. This result therefore implies that the change in the electron distribution of pyridine molecule under the electric field significantly depends on the adsorption sites on the Ag_{20} cluster. However, this discrepancy may be relatively unclear in experimental resonance Raman spectra, because the S- and V-complexes are mixed due to the near-degenerate energies.

B. Resonance Raman spectrum enhancement of pyridine on Ag_n (n = 5, 10 and 20) complexes

Next, let us look into the resonance Raman spectrum enhancement for the S- and V-complexes of pyridine molecule on Ag_5, Ag_{10} and Ag_{20} (pyridine@Ag_5, pyridine@Ag_{10}, and pyridine@Ag_{20}) clusters, of which the optimized structures are shown in Fig. 1. Figure 3 illustrates the resonance Raman enhancement factors of pyridine@Ag_{20} cluster for the S- and V-complexes with the incident light wavelengths corresponding to the CT excitations, which are calculated using three types of functionals: BLYP, B3LYP and LC-BLYP. The figure shows that the calculated chemical enhancement factors become up to 10^{12}, though they seriously depend on the functional used. Note that these huge enhancement factors are consistent with the experimental results.[5] Therefore, this result indicates that the huge enhancement factors in SERS can be explained by the resonance Raman spectroscopy for, at least, this small silver cluster. The significant dependence on the functional is interpreted by the reproducibility of the CT excitation energies. As mentioned in Sec. I, TDKS calculations tend to underestimate CT excitation energies and this underestimation is clearly solved by incorporating LC.[18,24] Actually, as the figure shows, the CT excitation wavelengths of the TDKS method are much shorter for LC-BLYP than those for BLYP and B3LYP. This is because the insufficient long-range exchange effects cause orbital mixings and consequently lead to the underestimation of the corresponding orbital energy gaps. In Fig. 3, the orbital mixings are found in the orbitals of the V-complex after CT for BLYP and B3LYP. This leads to the overestimation of the resonance Raman peak intensities, because it causes the

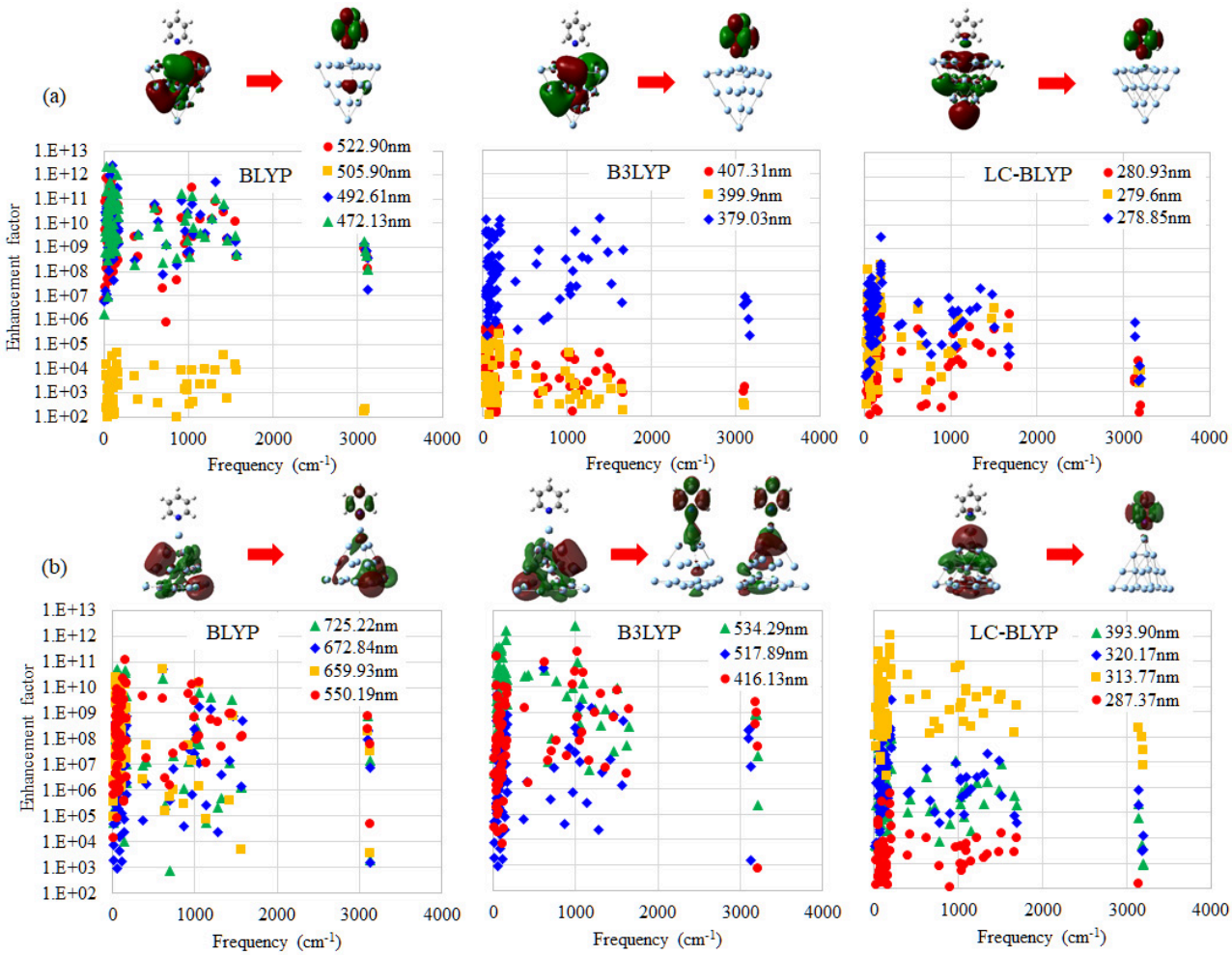

FIG. 3: The enhancement factors of surface-enhanced Raman spectroscopy for (a) the S-complex and (b) the V-complex of pyridine@Ag_{20} with respect to the vibrational frequency. These chemical enhancement factors are calculated as the ratios of the resonance Raman peak intensities to the off-resonance ones. The resonance Raman spectra are calculated for the incident light wavelengths corresponding to several low-lying charge transfer excitations, which are calculated in time-dependent Kohn-Sham calculations, as shown in the explanatory notes. BLYP, B3LYP and LC-BLYP functionals are used with the cc-pVDZ basis. The images of the molecular orbitals, which mainly contribute to these charge transfer excitations, are also shown for each functional.

serious underestimation of CT excitation energies, as shown in the longer CT wavelengths, and consequently the overestimation of the differential scattering cross sections in Eq. (1). Note that the SERS enhancement experimentally takes place by the photoirradiation of the wavelength around 406.7 nm on silver surface.[48] This wavelength is very close to the lowest

CT excitation energy of the V-complex, i.e., 393.90 nm. Although the chemical enhancement factors for this lowest excitation are smaller than those of 313.77 nm, the enhancement factor values, i.e., 10^7, are large enough to explain the experimental huge enhancements. Therefore, this experimental value supports the high reliability of the present calculations. Base on these results, it is concluded that long-range exchange effects should be incorporated to perform DFT calculations of resonance Raman spectra.

To investigate the cluster-size dependence, the chemical enhancement factors of the pyridine@Ag_{10} and pyridine@Ag_5 clusters are also calculated. Figures 4 and 5 display the resonance Raman enhancement factors of the pyridine@Ag_{10} and pyridine@Ag_5 clusters, respectively, for the S- and V-complexes. The figures show that the chemical enhancement factors are large enough even for these small clusters in the case of the V-complexes. This indicates that the resonance Raman enhancement factors hardly depend on the size of silver clusters for the V-complexes. The figures also suggest that the chemical enhancement factors of the S-complexes are much smaller than those of the V-complexes in LC-BLYP calculations. Since the mixing ratios of the S-complexes may increase due to the smaller energy difference from the V-complexes, i.e., 0.32 and 3.70 kcal/mol for Ag_{10} and Ag_5, respectively, the chemical enhancement factors of these clusters may be slightly smaller than that of Ag_{20} cluster. It is meaningful to note that Ag_5 has an open-shell electronic structure in contrast to the closed-shell ones of Ag_{20} and Ag_{10}. This result indicates that the resonance Raman activity hardly depends on the difference of open- and closed-shell electronic structures. Raman spectrum peaks essentially depend on the polarizability derivatives in terms of the vibration modes. Therefore, the Raman peaks are not directly affected by this difference as supported by theoretical studies on the resonance Raman activities of pyridine and very small metal clusters.[46] Based on these results, it is concluded that the huge enhancement factors of pyridine molecule on small silver clusters mainly come from the resonance Raman activity effects independent of the size of silver clusters.

C. Surface plasmon of Ag_{20} cluster

Finally, we explored the field enhancement effect, which is often called "surface plasmon effect", in order to compare the resonance Raman and surface plasmon effects on the enhancement factors of the Raman spectrum. Based on electrodynamics, the enhancement

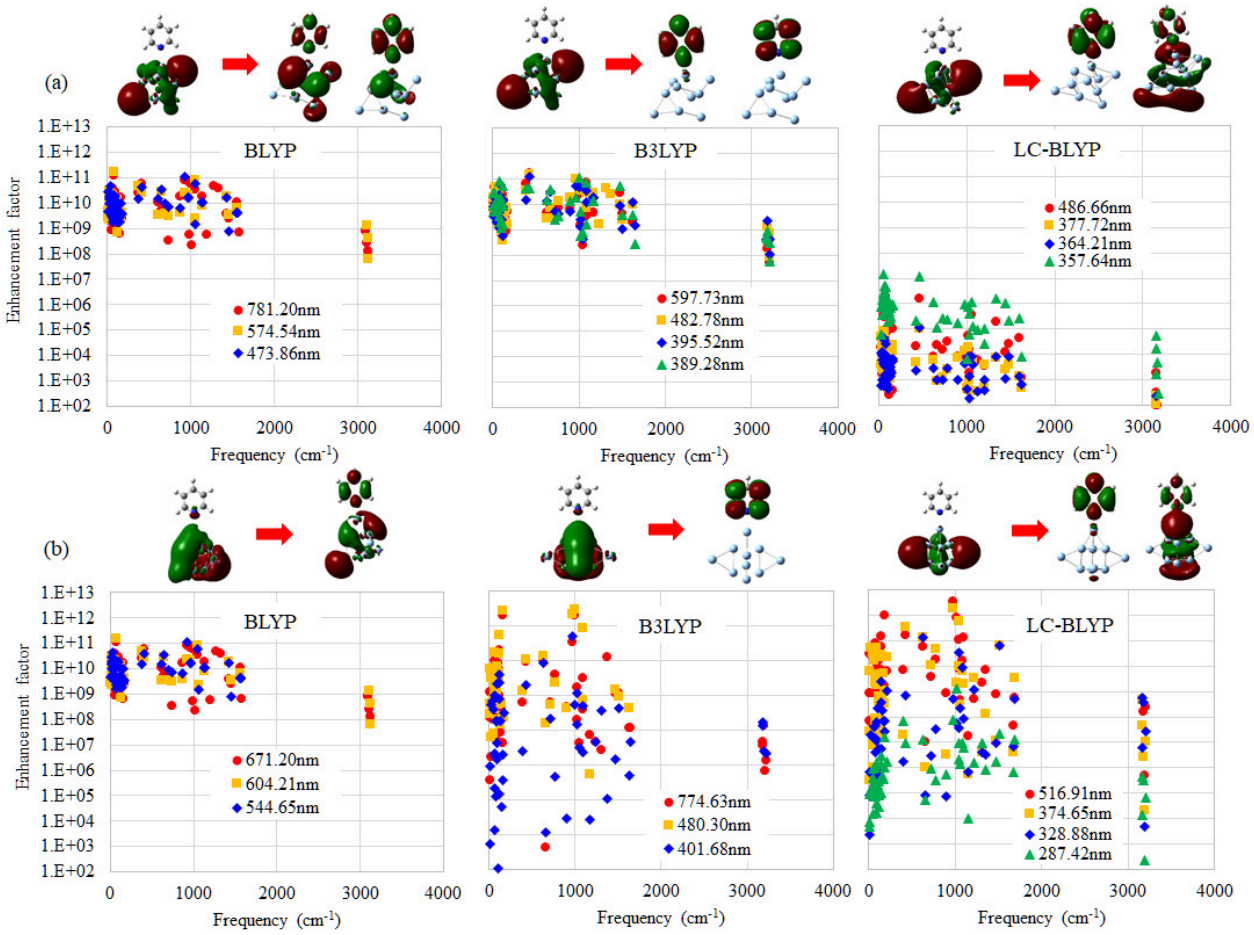

FIG. 4: The enhancement factors of surface-enhanced Raman spectroscopy for (a) the S-complex and (b) the V-complex of pyridine@Ag_{10} with respect to the vibrational frequency. These chemical enhancement factors are calculated as the ratios of the resonance Raman peak intensities to the off-resonance ones. The resonance Raman spectra are calculated for the incident light wavelengths corresponding to several low-lying charge transfer excitations, which are calculated in time-dependent Kohn-Sham calculations, as shown in the explanatory notes. BLYP, B3LYP and LC-BLYP functionals are used with the cc-pVDZ basis. The images of the molecular orbitals, which mainly contribute to these charge transfer excitations, are also shown for each functional.

of the electric field is calculated for the Ag_{20} cluster. Equation (7) indicates that the field enhancement is evaluated by the static and dynamic polarizabilities of the system under the pre-resonance condition. The absorption spectrum of Ag_{20} is shown in Fig. 6a. As the figure shows, the strongest absorption peak intensity is given at 3.55 eV. Figure 6b displays the polarizability around this peak. The figure indicates that the polarizability approaches

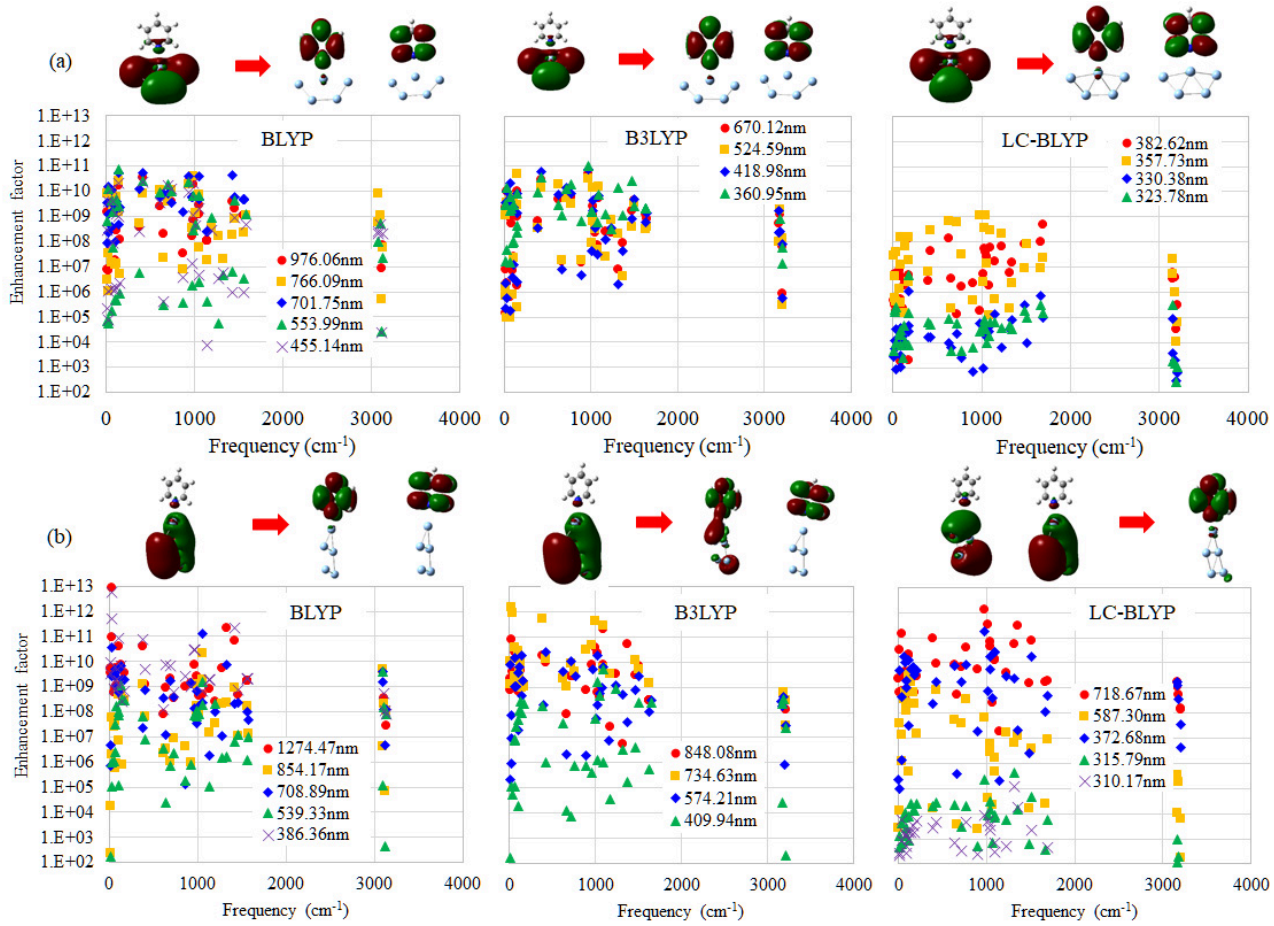

FIG. 5: The enhancement factors of surface-enhanced Raman spectroscopy for (a) the S-complex and (b) the V-complex of pyridine@Ag_5 with respect to the vibrational frequency. These chem-ical enhancement factors are calculated as the ratios of the resonance Raman peak intensities to the off-resonance ones. The resonance Raman spectra are calculated for the incident light wavelengths corresponding to several low-lying charge transfer excitations, which are calculated in time-dependent Kohn-Sham calculations, as shown in the explanatory notes. BLYP, B3LYP and LC-BLYP functionals are used with the cc-pVDZ basis. The images of the molecular orbitals, which mainly contribute to these charge transfer excitations, are also shown for each functional.

200,000 a.u. (i.e., $bohr^3$) under the pre-resonance condition. Note that the real part of the polarizability becomes zero under the resonance condition.

Under the resonance condition considering the lifetime of this excited state, the polarizability is roughly expressed by $2|\mu_{\rm res}|^2$,[49,50] where $\mu_{\rm res}$ is the transition dipole moment of an excited state. Since the lifetime of an excited state can be incorporated as a damping fac-

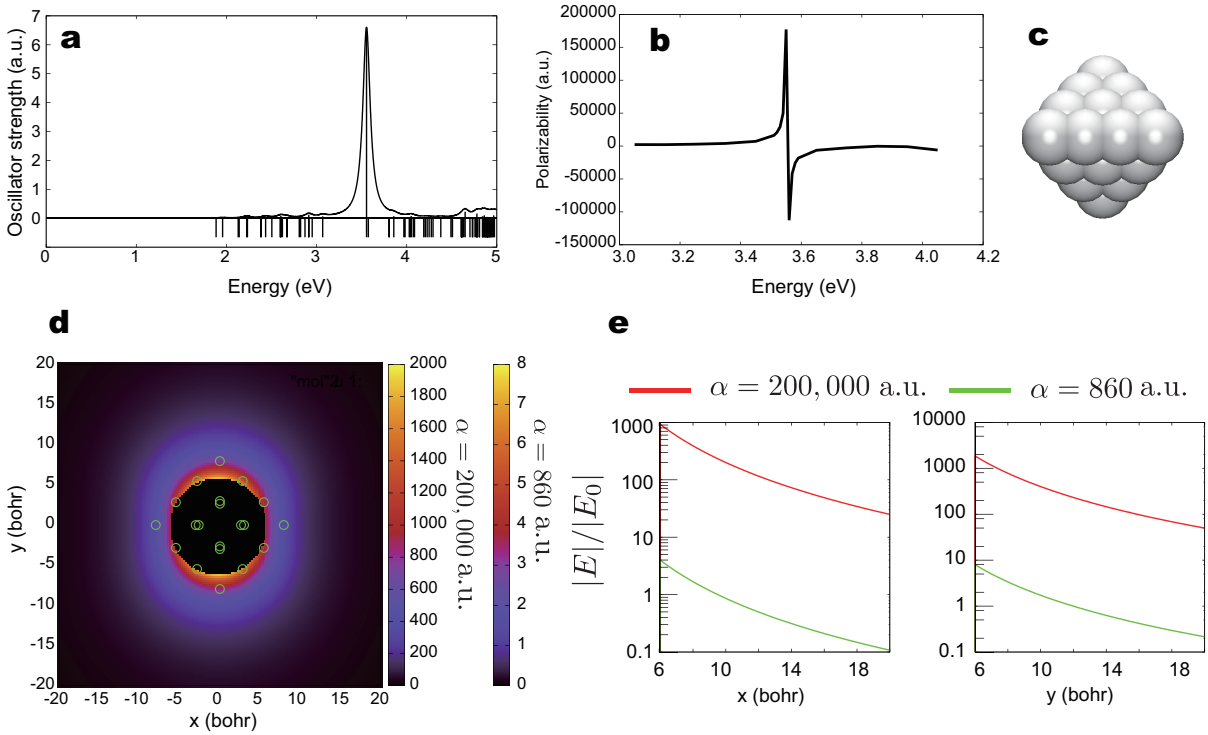

FIG. 6: (a) The simulated absorption spectrum of Ag_{20} calculated at RI-B3LYP/def-SV(P) level of theory. The lines below 0 show the position of excited states. Line spectrum is convoluted by Lorentzian of 0.05 eV. (b) The polarizability of Ag_{20} in the atomic unit (a.u.). (c) The space filling model of Ag_{20}. (d) The intensity map of dipole field relative to the incident electric field, $|E/E_0|$. The intensity around the center of mass of Ag_{20}, in which the intensity at the radius of 6 bohr is taken to be zero for visibility and the positions of the Ag atoms projected onto the xy plane are shown as the green circles. Color scales of the intensity are shown for $\alpha = 200,000$ a.u. in the left side and for $\alpha = 860$ a.u. in the right side. (e) The cross sections of $|E/E_0|$ along the x and y with $y = 0$ and $x = 0$, respectively.

tor in the imaginary part of the response function, the imaginary parts of the polarizability, $2|\mu_{\rm res}|^2$, are numerically calculated as the multiplication of the Lorentz function, of which the maximum value is unity.[51] However, it is not yet implemented in the present official version of TURBOMOLE.[42] The field enhancement is, therefore, evaluated neglecting the lifetime by the polarizability under the pre-resonance condition, as well as the static polarizability Figure 6d shows the intensity map of the calculated dipole field relative to the incident electric field in Eq. (7) for the dynamic and static polarizabilities. The corresponding cross sections along the x and y axes are also shown in Fig. 6e. Since the vertex atom of Ag_{20}

is located around 8 bohr far from the center of mass, the field enhancement becomes $< 10^3$ even using the polarizability under the pre-resonance condition and ≤ 1 for the use of the static polarizability. Using Eq. (7), the field enhancement is also roughly estimated around the surface of the cluster. Assuming that the distance from the center of mass to the surface is 10 bohr for the Ag_{20} cluster, the enhancement factor is roughly evaluated as the order of $\sim \alpha(\omega)/1000$ at the surface of the cluster. Since the static and dynamic polarizabilities are calculated as ∼860 a.u. and ∼200,000 a.u., respectively, at the strongest absorption energy (3.55 eV), the enhancement is evaluated as < 1 for the static field and as ∼200 for the dynamic field under this assumption. Though the enhancement for the dynamic field (∼200) is too large to be compared to the enhancement values in the previous studies,[51,52] we should notice that this calculation neglects the lifetime, indicating that the lifetime is set to be infinite.[53,54] The dynamic polarizability is represented as[54]

$$\tilde{\alpha}_{\alpha\beta} = \sum_{m'} \frac{\langle f \left|\mu_\alpha\right| m' \rangle \langle m' \left|\mu_\beta\right| i \rangle}{\omega_{mi} - \omega - i\gamma}, \tag{9}$$

where $\langle f \mid$ and $\mid i \rangle$ are the final and initial vibrational states, respectively, and $\omega_{mi} = \omega_m - \omega_i$ is the energy difference between the middle anad initial states, μ_α and μ_β are the Cartesian components, i.e., $(\alpha, \beta) = (x, y, z)$, of the transition dipole moments between the ground and excited states, and m' is the vibrational states of the corresponding excited state. What we should notice is that Eq. (9) contains the damping constant for the corresponding excited state, γ, which is interpreted as the lifetime of the excited state. Since the large dynamic polarizability stems from its small denominator, the lifetime significantly contributes to the enhancement factors. The neglect of lifetime, therefore, causes the overestimation of the surface plasmon effect on SERS. This result, therefore, does not indicate the significant surface plasmon effect on SERS but rather cautions that the lifetime should be considered to evaluate the surface plasmon effects.

It is, therefore, concluded that the electromagnetic surface plasmon effect on the enhancement factor of the Raman spectrum is much smaller than the resonance Raman activity effect for small silver nanoclusters. This conclusion is consistent with an experimental observation of the SERS effect on sub-nanometer metal nanoclusters consisting of two through eight silver atoms.[55]

IV. CONCLUSIONS

In this study, we have investigated the cause for the enhancement factors of surface-enhanced Raman spectroscopy (SERS) by the addition of small silver nanoclusters. This study focuses on the significance of the resonance Raman activity and the surface plasmon effects on SERS. Silver nanoclusters are known to dramatically enhance the Raman scattering cross section of adsorbed molecules by 10^7 through 10^{12} times, which pave the way for single-molecule spectroscopy and microscopy. The surface plasmon effect on incident light has often been interpreted as the main cause for this enhancement. However, the cause for the huge SERS enhancement has rarely been investigated by comparing the resonance Raman activity and surface plasmon effects on SERS.

To make it clear, we have first explored the resonance and off-resonance Raman spectra for the complexes of pyridine molecule attaching three small silver nanoclusters, i.e., Ag_5, Ag_{10} and Ag_{20}, for the surface (S) and vertex (V) complexes. The resonance Raman activities have been calculated using the incident light wavenumbers of the charge transfer (CT) excitations of the response time-dependent Kohn-Sham (TDKS) method, which give the most enhanced Raman spectrum peaks for each complex. As a result, we found that the resonance Raman spectrum peaks are dramatically increased by incorporating the incident radiation and provide very different features for the S- and V-complexes in contrast to very similar features in the off-resonance Raman spectra. This indicates that the resonance Raman activities and also the electron distribution variance under the electric field significantly depend on the adsorption sites, though these dependences are unclear in experimental spectra due to the mixing of adsorption types.

We have, next, studied the resonance Raman enhancement factors for the same complexes using the incident light wavenumbers corresponding to several low-lying CT excitation energies. The calculated results of the pyridine@Ag_{20} complex show that the chemical enhancement factors become up to 10^{12}, though they significantly depend on the functional used. This indicates that the huge enhancement factors of SERS can be explained by the resonance Raman effect for, at least, small silver nanoclusters. The results also show that the long-range correction tends to decrease the chemical enhancement factors by correctly reducing the orbital mixings. For investigating the cluster-size dependence, we have also calculated the chemical enhancement for the pyridine@Ag_5 and pyridine@Ag_{10} complexes.

The results show that the chemical enhancement factors are huge for the V-complexes of even these small clusters, while they significantly depend on the functional used for the S-complexes. It is, therefore, concluded that the huge enhancement factors come from the resonance Raman activity effects for, at least, the inclusion of small silver nanoclusters.

To confirm the above conclusion, we have finally examined the electromagnetic field enhancement effects, "surface plasmon effect", of the Ag_{20} cluster for the strongest absorption peak. The calculated intensity map of dipole field relative to the incident electric field shows that the field enhancement is less than 10^3 even using the polarizability under the pre-resonance condition and < 1 for the static polarizability. The roughly-evaluated enhancement factors of dipole moments are < 1 for the static field and $\sim$200 for the dynamic field at the strongest absorption energy. Since the considerable enhancement for the dynamic field is considered to come from the neglect of the lifetime for staying in the excited state, it is confirmed that the resonance Raman activity effect is dominant in the SERS enhancement factors for, at least, small silver nanoclusters.

ACKNOWLEDGMENTS

This research was supported by the Japanese Ministry of Education, Culture, Sports, Science and Technology (MEXT) (Grants: 17H01188, 16KT0047, and 17K14428). This study was also partly supported by MEXT as "Priority Issue on Post-K computer" (Development of new fundamental technologies for high-efficiency energy creation, conversion/storage and use). Institute for Chemical Reaction Design and Discovery (ICReDD) was established by World Premier International Research Initiative (WPI), MEXT, Japan.

SUPPLEMENTARY MATERIAL AVAILABLE

The Cartesian coordinates of the optimized geometries of pyridine@Ag_{20}, pyridine@Ag_{10} and pyridine@Ag_5 complexes are given for the S- and V-complexes in the supporting information. For the pyridine@Ag_{20} complex, the MO transitions and their coefficients in the response functions of the TDKS excitations corresponding to the low-lying charge transfer excitations are also listed with the wavelenths and the oscillator strengths. This material is available free of charge via the Internet at xxxx.

FIGURE CAPTIONS

Fig. 1.
Optimized geometries of silver cluster models, Ag_5, Ag_{10} and Ag_{20}, attaching pyridine molecule for the S- and V-complex structures with the energy differences. LC-BLYP/cc-pVDZ is used.

Fig. 2.
Calculated on/off-resonance Raman spectra of pyridine@Ag_{20} complexes: (a) and (b) correspond to the off-resonance Raman spectra of pyridine molecule and Ag_{20} cluster, (c) and (d) correspond to the off-resonance Raman spectra of the S- and V-complexes and (e) and (f) correspond to the resonance ones of the S- and V-complexes, respectively. All the peaks are multiplied by the Gaussian distribution function. For (e) and (d), the spectra correspond to the lowest charge transfer excitations of the complexes, for which the wavelengths of 280.93 and 393.90 nm for S- and V-complexes, respectively. LC-BLYP/cc-pVDZ is used.

Fig. 3.
The enhancement factors of surface-enhanced Raman spectroscopy for (a) the S-complex and (b) the V-complex of pyridine@Ag_{20} with respect to the vibrational frequency. These chemical enhancement factors are calculated as the ratios of the resonance Raman peak intensities to the off-resonance ones. The resonance Raman spectra are calculated for the incident light wavelengths corresponding to several low-lying charge transfer excitations, which are calculated in time-dependent Kohn-Sham calculations, as shown in the explanatory notes. BLYP, B3LYP and LC-BLYP functionals are used with the cc-pVDZ basis. The images of the molecular orbitals, which mainly contribute to these charge transfer excitations, are also shown for each functional.

Fig. 4.
The enhancement factors of surface-enhanced Raman spectroscopy for (a) the S-complex and (b) the V-complex of pyridine@Ag_{10} with respect to the vibrational frequency. These chemical enhancement factors are calculated as the ratios of the resonance Raman peak intensities to the off-resonance ones. The resonance Raman spectra are calculated for the incident light wavelengths of several low-lying charge transfer excitations, which are shown

in the explanatory notes. BLYP, B3LYP and LC-BLYP functionals are used with the cc-pVDZ basis. The images of the molecular orbitals, which mainly contribute to these charge transfer excitations, are also shown for each functional.

Fig. 5.

The enhancement factors of surface-enhanced Raman spectroscopy for (a) the S-complex and (b) the V-complex of pyridine@Ag_5 with respect to the vibrational frequency. The resonance Raman spectra are calculated for the incident light wavelengths of several low-lying charge transfer excitations, which are shown in the explanatory notes. BLYP, B3LYP and LC-BLYP functionals are used with the cc-pVDZ basis. The images of the molecular orbitals, which mainly contribute to these charge transfer excitations, are also shown for each functional.

Fig. 6.

(a) The simulated absorption spectrum of Ag_{20} calculated at RI-B3LYP/def-SV(P) level of theory. The lines below 0 show the position of excited states. Line spectrum is convoluted by Lorentzian of 0.05 eV. (b) The polarizability of Ag_{20} in the atomic unit (a.u.). (c) The space filling model of Ag_{20}. (d) The intensity map of dipole field relative to the incident electric field, $|E/E_0|$. The intensity around the center of mass of Ag_{20}, in which the intensity at the radius of 6 bohr is taken to be zero for visibility and the positions of the Ag atoms projected onto the xy plane are shown as the green circles. Color scales of the intensity are shown for $\alpha = 200,000$ a.u. in the left side and for $\alpha = 860$ a.u. in the right side. (e) The cross sections of $|E/E_0|$ along the x and y with $y = 0$ and $x = 0$, respectively.

* Electronic address: tsuneda@phoenix.kobe-u.ac.jp

[1] R. H. Ritchie, Phys. Rev. **106**, 874 (1957).

[2] W. L. Barnes, A. Dereux, and T. W. Ebbesen, Nature **424**, 824 (2003).

[3] L. Novotny and B. Hecht, Principles of Nano-Optics (Cambridge University Press, New York, 2006).

[4] S. A. Maier, Plasmonics: Fundamentals and Applications (Springer US, New York, 2007).

[5] D. Sarid and W. A. Challener, Modern Introduction to Surface Plasmons: Theory, Mathematica Modeling, and Applications (Cambridge University Press, 2010).

[6] E. Ozbay, Science **311**, 189 (2006).

[7] H. Imada, K. Miwa, M. Imai-Imada, S. Kawahara, K. Kimura, and Y. Kim, Phys. Rev. Lett. **119**, 013901 (2017).

[8] E. Kazuma, J. Jung, H. Ueba, M. Trenary, and Y. Kim, Science **360**, 521 (2018).

[9] E. Kazuma and Y. Kim, Angew. Chemie Int. Ed. **58**, 2 (2019).

[10] L. Jensen, C. M. Aikens, and G. C. Schatz, Chem. Soc. Rev. **37**, 1061 (2008).

[11] S. M. Morton, D. W. Silverstein, and L. Jensen, Chem. Rev. **111**, 3962 (2011).

[12] M. Fleischmann, P. J. Hendra, and A. J. McQuillan, Chem. Phys. Lett. **26**, 163 (1974).

[13] W.-H. Yang, G. C. Schatz, and R. P. Van Duyne, J. Chem. Phys. **103**, 869 (1995).

[14] K. S. Yee, IEEE Trans. Antennas Propag. **AP-14**, 302 (1966).

[15] M. Futamata, Y. Maruyama, and M. Ishikawa, J. Phys. Chem. B **107**, 7607 (2003).

[16] L. Zhao, L. Jensen, and G. C. Schatz, J. Am. Chem. Soc. **128**, 2911 (2006).

[17] T. Higaki, M. Zhou, K. J. Lambright, K. Kirschbaum, M. Y. Sfeir, and R. Jin, J. Am. Chem. Soc. **140**, 5691 (2018).

[18] T. Tsuneda and K. Hirao, in Theoretical and Quantum Chemistry at the 21st Century Dawn End, edited by T. Chakraborty and R. Carbo (Apple Academic Press, Florida, 2018), pp. 153–195.

[19] N. A. Sakthivel, M. Stener, L. Sementa, A. Fortunelli, G. Ramakrishna, and A. Dass, J. Phys. Chem. Lett. **9**, 1295 (2018).

[20] X.-B. Xu, Z. Yi, Y.-Y. Wang, X. Geng, J.-S. Luo, B.-C. Luo, Y.-G. Yi, and Y.-J. Tang, J. Phys. Chem. C **116**, 24046 (2012).

[21] T. Tsuneda and K. Hirao, WIREs Comput. Mol. Sci. **4**, 375 (2014).

[22] H. Iikura, T. Tsuneda, T. Yanai, and K. Hirao, J. Chem. Phys. **115**, 3540 (2001).

[23] T. Tsuneda, J.-W. Song, S. Suzuki, and K. Hirao, J. Chem. Phys. **133**, 174101 (2010).

[24] Y. Tawada, T. Tsuneda, S. Yanagisawa, T. Yanai, and K. Hirao, J. Chem. Phys. **120**, 8425 (2004).

[25] D. W. Silverstein and L. Jensen, J. Chem. Theory Comput. **6**, 2845 (2010).

[26] T. Tsuneda, J. Comput. Chem. **40**, 206 (2018).

[27] J. P. Perdew, K. Burke, and M. Ernzerhof, Phys. Rev. Lett. **77**, 3865 (1996).

[28] W. Kohn and L. J. Sham, Phys. Rev. A **140**, 1133 (1965).

[29] T. Tsuneda, Density Functional Theory in Quantum Chemistry (Springer, Tokyo, 2014).

[30] A. D. Becke, Phys. Rev. A **38**, 3098 (1988).

[31] C. Lee, W. Yang, and R. G. Parr, Phys. Rev. B **37**, 785 (1988).

[32] A. D. Becke, J. Chem. Phys. **98**, 5648 (1993).

[33] T. H. Dunning Jr., J. Chem. Phys. **90**, 1007 (1989).

[34] R. A. Kendall, J. T. H. Dunning, and R. J. Harrison, J. Chem. Phys. **96**, 6796 (1992).

[35] P. J. Hay and W. R. Wadt, J. Chem. Phys. **82**, 299 (1985).

[36] J. Neugebauer, M. Reiher, C. Kind, and B. A. Hess, J. Comput. Chem. **23**, 895 (2002).

[37] M. J. Frisch, G. W. Trucks, H. B. Schlegel, G. E. Scuseria, M. A. Robb, J. R. Cheeseman, G. Scalmani, V. Barone, B. Mennucci, G. A. Petersson, et al., Gaussian09 Revision D.01 (2009), gaussian Inc. Wallingford CT.

[38] R. Dennington, T. Keith, and J. Millam, Gaussview, version 5 (2009), semichem Inc., Shawnee Mission KS.

[39] J. D. Jackson, Classical Electrodynamics Third Edition (Wiley, 1998).

[40] A. Schäfer, H. Horn, and R. Ahlrichs, J. Chem. Phys. **97**, 2571 (1992).

[41] K. Eichkorn, F. Weigend, O. Treutler, and R. Ahlrichs, Theor. Chem. Acc. **97**, 119 (1997).

[42] Turbomole v7.3 2018, a developtment of University of Karlsruhe and Forschungszentrum Karlsruhe GmbH, 1989-2007, TURBOMOLE GmbH, since 2007; available from http://www.turbomole.com.

[43] R. Ahlrichs, M. Bär, M. Häser, H. Horn, and C. Kölmel, Chem. Phys. Lett. **162**, 165 (1989).

[44] J. F. Arenas, I. L. Tocon, J. C. Otero, and J. I. Marcos, J. Phys. Chem. **100**, 9254 (1996).

[45] D.-Y. Wu, M. Hayashi, S.-H. Lin, and Z.-Q. Tian, Spectrochim. Acta A **60**, 137 (2004).

[46] D.-Y. Wu, X.-M. Liu, S. Duan, X. Xu, B. Ren, S.-H. Lin, and Z.-Q. Tian, J. Phys. Chem. C

112, 4195 (2008).

[47] R. L. Birke, V. Znamenskiy, and J. R. Lombardi, J. Chem. Phys. **132**, 214707 (2010).

[48] Y. Kitahama and Y. Ozaki, Analyst **141**, 5020 (2016).

[49] S. Mukamel, Principles of Nonlinear Optical Spectroscopy, Oxford Series on Optical and Imaging Sciences (Oxford University Press, 1999).

[50] R. W. Boyd, Nonlinear Optics, Third Edition (Academic Press, 2008).

[51] L. Jensen, J. Autschbach, and G. C. Schatz, J. Chem. Phys. **122**, 224115 (2005).

[52] E. J. Zeman and G. C. Schatz, J. Phys. Chem. **91**, 634 (1987).

[53] A. Baiardi, J. Bloino, and V. Barone, J. Chem. Phys. **141**, 114108 (2014).

[54] F. Egidi, J. Bloino, C. Cappelli, and V. Barone, J. Chem. Theory Comput. **10**, 346 (2014).

[55] L. Peyser-Capadona, J. Zheng, J. I. González, T.-H. Lee, S. A. Patel, and R. M. Dickson, Phys. Rev. Lett. **94**, 058301 (2005).